Supporting Information

In-situ Synthesis of a Low-PtCo @ Porous Carbon Catalyst for Highly Efficient Hydrogen Evolution Reaction

Yudao Qin[†], Xiaoyu Han[†], Srinivas Gadipelli[†], Jian Guo[†], Shijie Wu[‡], Liqun Kang[§], June Callison[†,‖] and Zhengxiao Guo*,[†]

[†]Department of Chemistry, University College London, 20 Gordon Street, London, WC1H 0AJ, UK.

[‡]Semiconductor Measurement Solutions, Keysight Technologies, Inc., Santa Clara, California 95051, United States.

[§]UK Catalysis Hub, Research Complex at Harwell (RCaH), Rutherford Appleton Laboratory, Harwell Oxon, OX11 0FA, UK.

[‖]Department of Chemical Engineering, University College London, Torrington Place, London, WC1E 7JE, UK.

*Corresponding authors: z.x.guo@ucl.ac.uk

List of Abbreviations

HER -Hydrogen evolution reaction

ZIFs -Zeolitic imidazolate frameworks

CPt@ZIF-8/CPt@ZIF-67- ZIF-8/ZIF-67 with Pt doping with carbonization at 900 °C for 6h.

CPt@ZIF-8-x°C-yh/ CPt@ZIF-67-x°C-yh - Carbonized platinum doped ZIF-8 or ZIF-67 at particular temperature, example 800 °C with a period of 6h CPt@ZIF-67-800C-6h (normally for 900°C-6 h carbonization condition unless otherwise specified, example, 2 h carbonized sample is identified as CPt@ZIF-67-900°C-2h)

PXRD - Powder X-ray diffraction

XPS - X-ray photoelectron spectroscopy

SEM - Scanning electron microscopy

TEM - Transmission electron microscopy

AFM - Atomic force microscopy

In order to minimise the dosage of noble metal Pt and maximise the surface area (active sites) of electrocatalysts, zeolite imidazole frameworks are applied. ZIF-8 and ZIF-67 are the first choices based on simplicity of synthesis, cheap reaction precursors and the existence of high electroconductive Zn or Co metals (Fig. S1a).[1]

Zeolitic imidazolate frameworks (ZIFs) are a subclass of metal organic frameworks (MOFs, also known as porous coordination polymers). ZIFs are also a class of porous crystals constructed from tetrahedral transition metal ions such as Zn and Co based on their linkage to imidazolate (Im). As shown in Fig. S1b, imidazolate displays a conjugate structure that gives a high electron density that may enhance electron transfer and conductivity. The synthesis procedure for ZIF-67 and ZIF-8 from 2-methylimidazole is illustrated in the experimental section.

In these ZIFs, the M-Im-M (M = metal) angle approaches 145°, giving them tetrahedral morphology. Notably, ZIFs exhibit permanent porosity and high thermal and chemical stability, which make them attractive candidates for use as the template for carbon-based materials. In comparison to the other MOFs, ZIFs share many rich elements of zeolite

chemistry in terms of both structural topologies and coordination factors. In addition, they feature exceptional thermal and chemical stability due to the fact that a cage-form to encapsulate the central reactive transition metal.[2] Although reactive nitrogen atoms exist in the imidazolate linker (Fig. S1b), the extra lone pair of nitrogen atoms are stabilised by the five-membered ring.
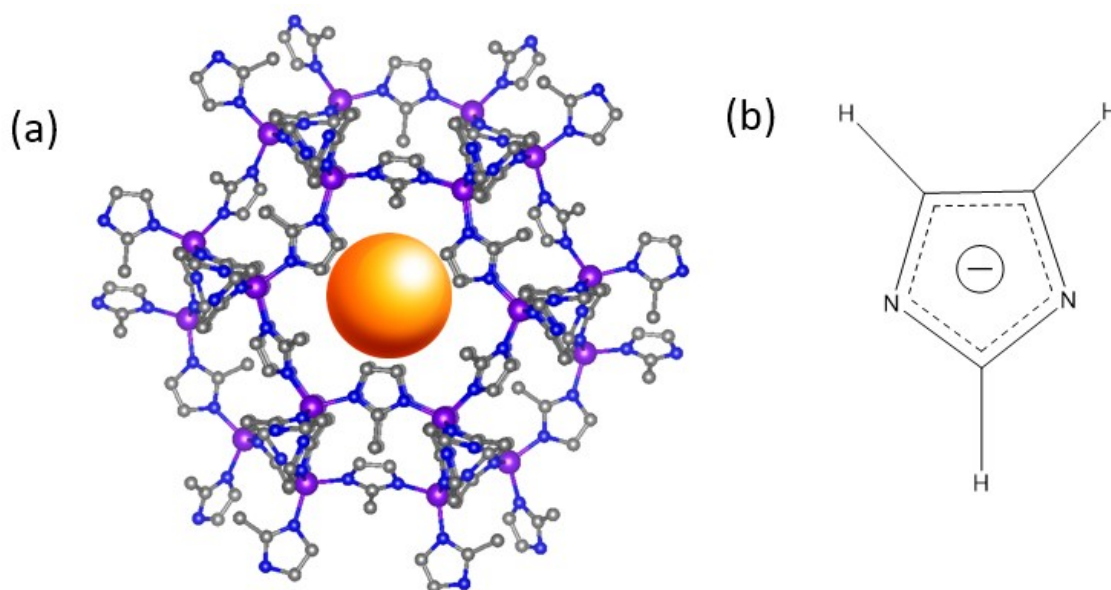

Fig. S1. (a) 3D structure of ZIF-67/ZIF-8 (grey ball = carbon atom, blue ball = nitrogen atom, purple ball = cobalt/zinc atom). (b) Molecular structure of imidazolate.

Both, ZIF-67 and ZIF-8 demonstrate a same permanent porosity of 58.8% (Table S2) and their surface areas are 1,320 m^2g^{-1} and 1,810 m^2g^{-1}, respectively. The surface areas are an order of magnitude higher than that of the 20 wt% Pt/C catalyst, which is only in the range of 10 to 200 m^2g^{-1}.[3]

Their extremely high stability, porosity, and surface area make ZIF-67 and ZIF-8 the best candidates for creating the template to maximise the distribution of Pt nanoparticles, improving reactivity and increasing the number of active sites of the catalyst. Carbonization is an effective technique of removing unwanted functional groups from the ZIF structures to achieve graphitic carbon support and electric conductivity. During high temperature carbonization over 1000 °C,

the purity exceeds 90% and the yield can be lower than 50%. If the carbonization temperature exceeds 900 ℃, the central metal zinc in ZIF-8 is virtually all released, as the boiling point of zinc is 907 ℃[4] yet cobalt (boiling point is 2927 ℃)[5] still remains. The correct balance therefore needs to be carefully determined. Both substances feature the properties of high electric conductivity and surface area, making them an ideal catalyst for HER at relatively low cost when compared with commercial 20 wt% Pt/C catalysts. Central metal cobalt in ZIF-67 also provides the enhancement of conductivity. The ZIF-67 and ZIF-8 share the same crystalline structure with the only difference in the linkage atom, Co and Zn, respectively (Fig. S1).
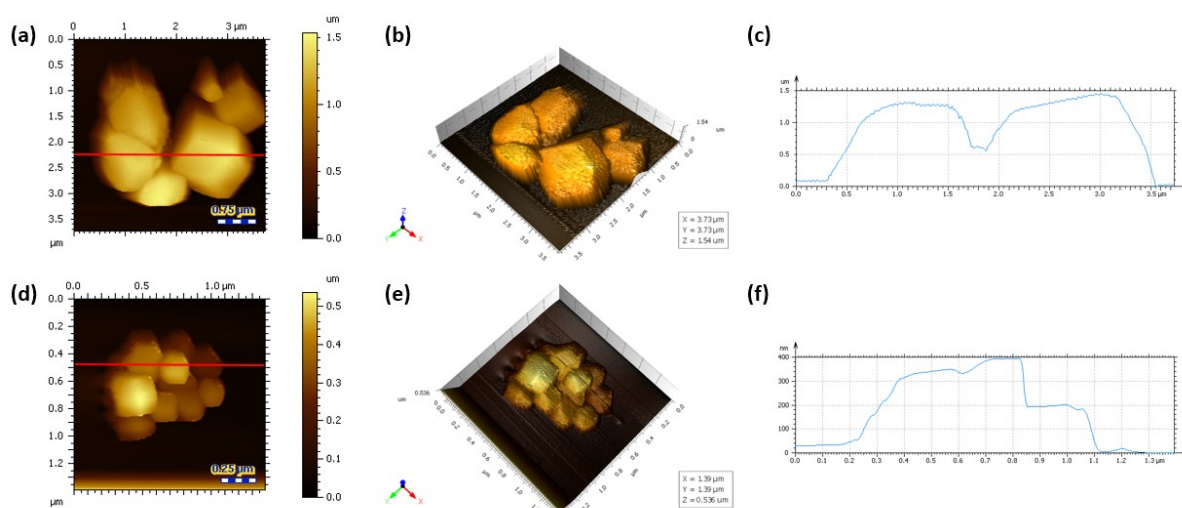

Fig. S2. (a) AFM image of Pt@ZIF-67. (b) 3D morphology of Pt@ZIF-67. (c) Height profile corresponding to the red line in (a). (d) AFM image of Pt@ZIF-8. (e) 3D morphology of Pt@ZIF-8. (f) Height profile corresponding to the red line in (d).
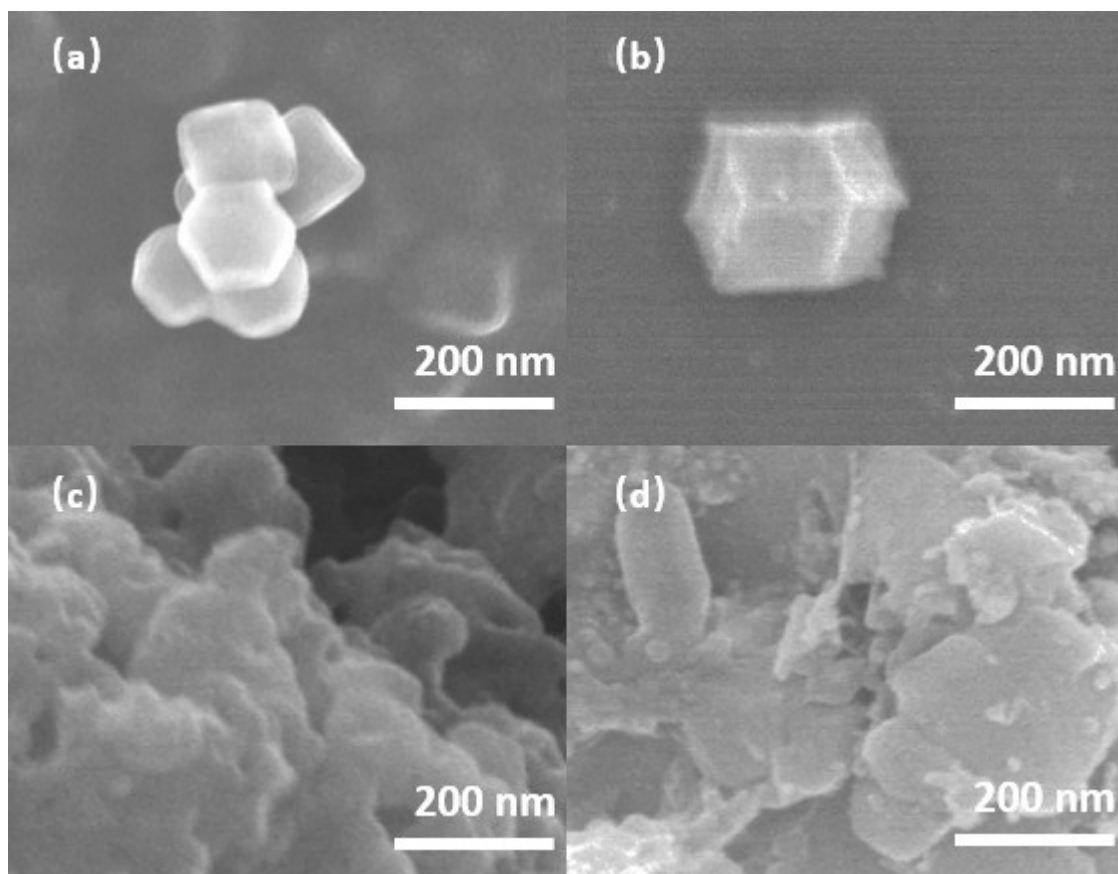
Fig. S3. SEM image of (a) Pt@ZIF-8, (b) Pt@ZIF-67, (c) CPt@ZIF-8, and (d) CPt@ZIF-67.
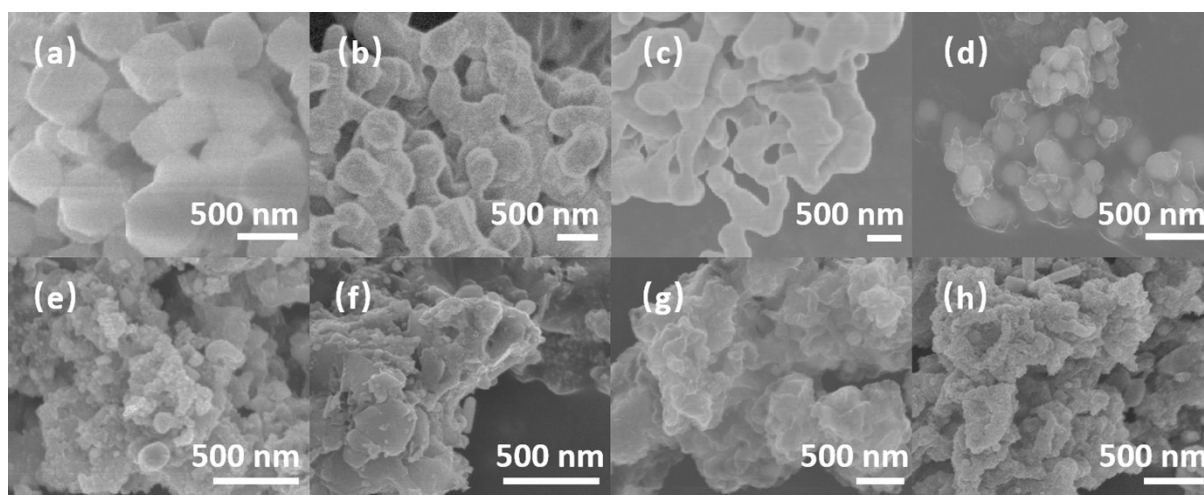

Fig. S4. SEM image of (a) ZIF-67, (b) CPt@ZIF-67-600C-2h, (c) CPt@ZIF-67-700C-2h, (d) CPt@ZIF-67-800C-2h, (e) CPt@ZIF-67-900C-2h, (f) CPt@ZIF-67-900C-6h, (g) CPt@ZIF-67-900C-6h, and (h) CPt@ZIF-67-1000C-2h.
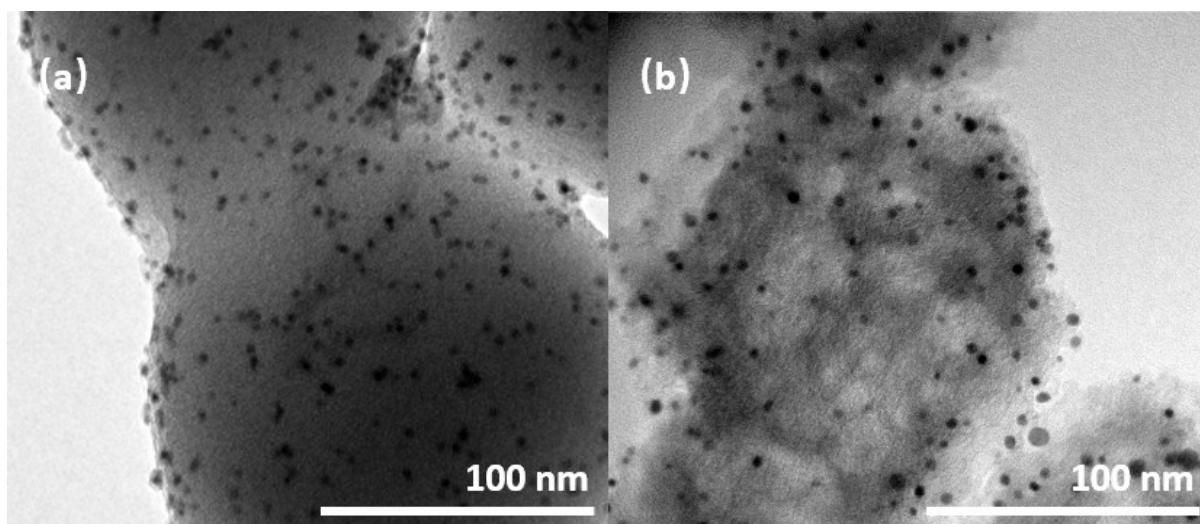
Fig. S5. TEM images for (a) as-synthesized Pt@ZIF-8, and (b) annealed CPt@ZIF-8.

TEM characterizations of Pt@ZIF-8 and CPt@ZIF-8 show the size and density of the metal clusters in ZIF-8 in Fig. S5a and S5b, respectively. Compared with the particle sizes in Fig. S5a, the Pt cluster size have doubled after the annealing CPt@ZIF-8, which suggest that Pt only particles tends to grow during annealing, due to Ostwald ripening with kinetic-limited growth.
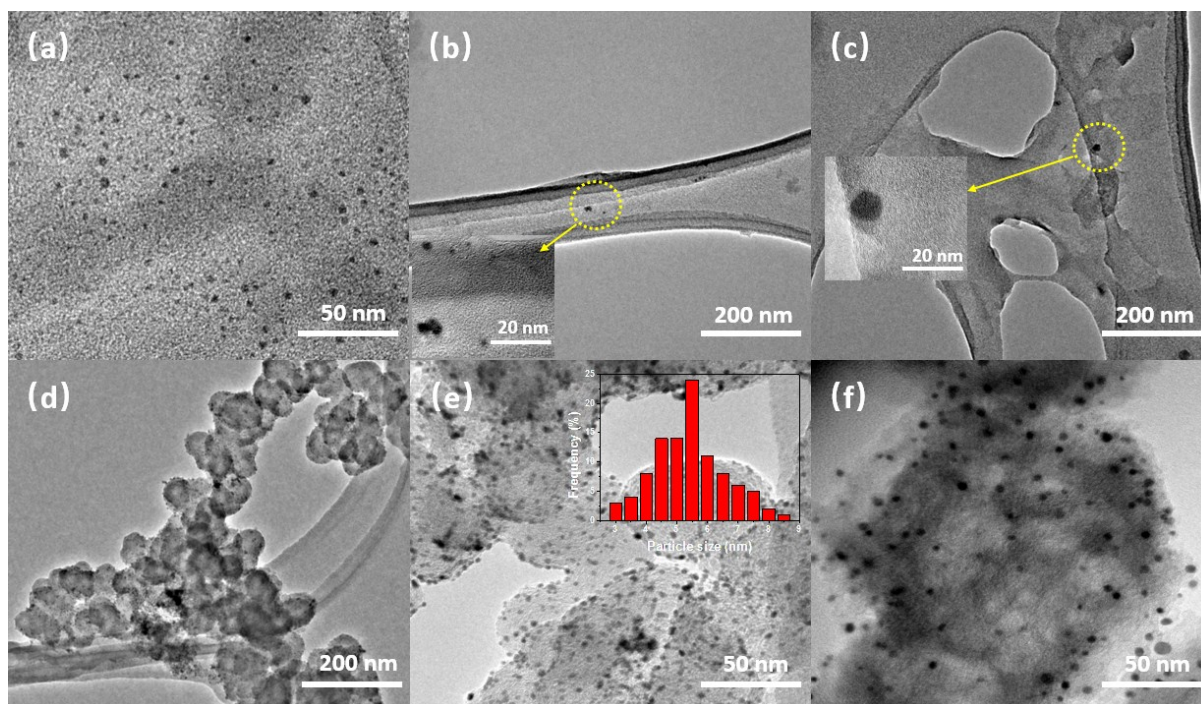
Fig. S6. TEM image of (a) metal nanoparticles deposited onto the carbon support for CPt@ZIF-67, (b) CPt@ZIF-67 nanoparticles in homogenous solution before electrochemical test and the inset shows the size of nanoparticles. (c) TEM image of CPt@ZIF-67 after 24h electrochemical stability test and the inset shows the size of nanoparticles remains after stability test. (d) TEM image of commercial 20 wt% Pt/C. (e) TEM image of commercial 20 wt% Pt/C and the inset shows the size distribution of nanoparticles for commercial 20 wt% Pt/C, it was analyzed by randomly selecting 100 nanoparticles to measure their diameters (average dimeter = 5.2 nm). (f) TEM image of metal nanoparticles deposited on to the carbon support for CPt@ZIF-8.
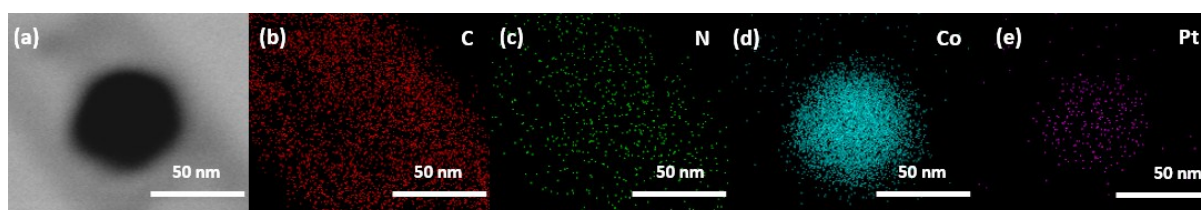

Fig. S7. (a) TEM image of Pt@ZIF-67. Element mappings of (b) carbon, (c) nitrogen, (d) cobalt, and (e) platinum.
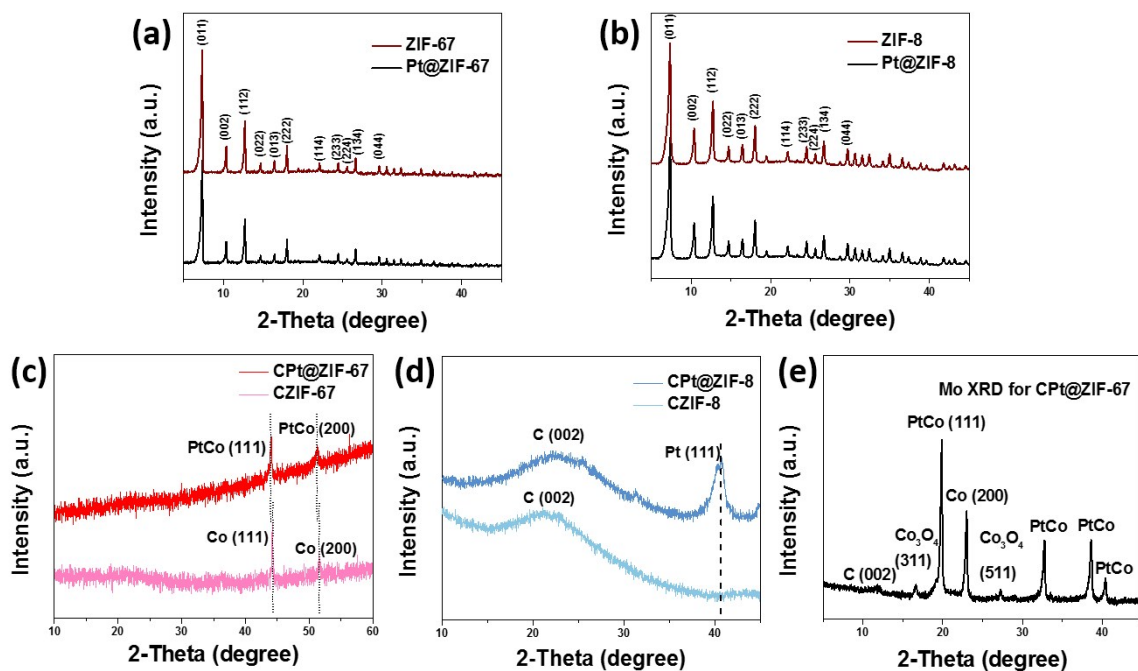
Fig. S8. The PXRD diffraction pattern of (a) ZIF-67 and Pt@ZIF-67, (b) PtZIF-8 and Pt@ZIF-8, (c) CPt@ZIF-67 and CZIF-67, (d) CPt@ZIF-8 and CZIF-8, under Cu radiation, and (e) CPt@ZIF-67 under Mo radiation.
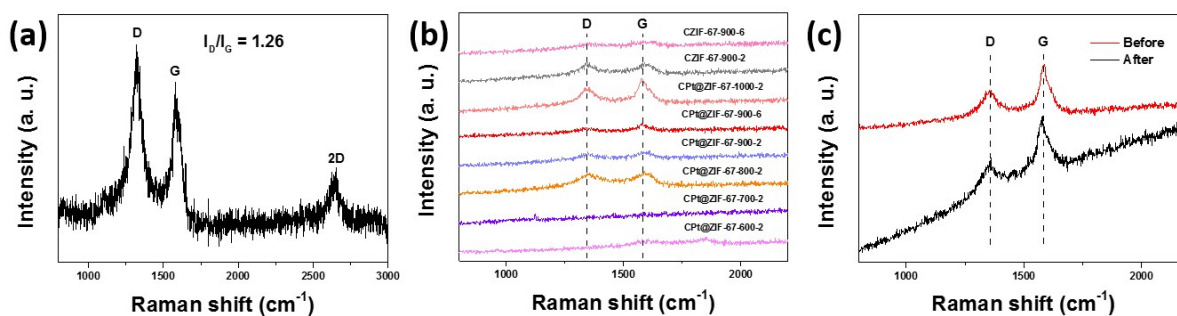

Fig. S9. Raman spectra of (a) CPt@ZIF-67, (b) CZIF-67-900-6, CZIF-67-900-2, C10Pt@ZIF-67-1000-2, C10Pt@ZIF-67-900-6, C10Pt@ZIF-67-900-2, C10PtZIF-67-800-2, C10PtZIF-67-700-2 and C10PtZIF-67-600-2. (c) Raman spectra of CPt@ZIF-67 before and after 24h electrochemical stability test. The peak D locates at 1340 cm^{-1}, the peak G locates at 1596 cm^{-1} and the 2D peak locates at 2652 cm^{-1}.
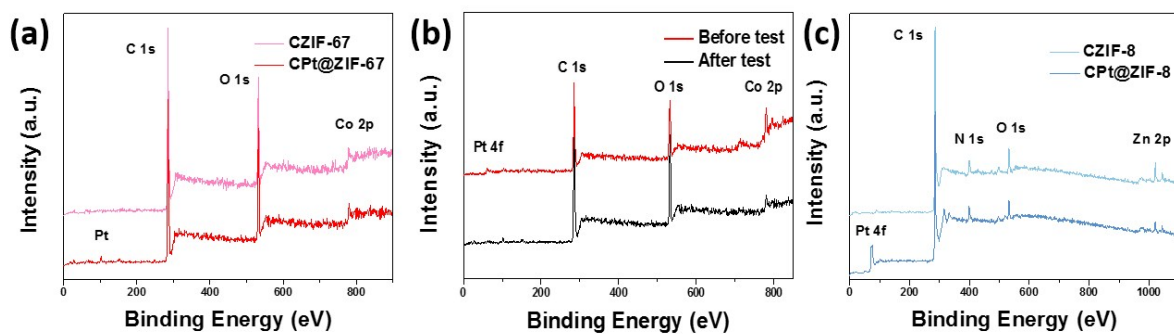
Fig. S10. XPS survey spectra of (a) CZIF-67 and CPt@ZIF-67, (b) CZIF-67 and CPt@ZIF-67 before and after 24h electrochemical stability test, (c) CZIF-8 and CPt@ZIF-8.
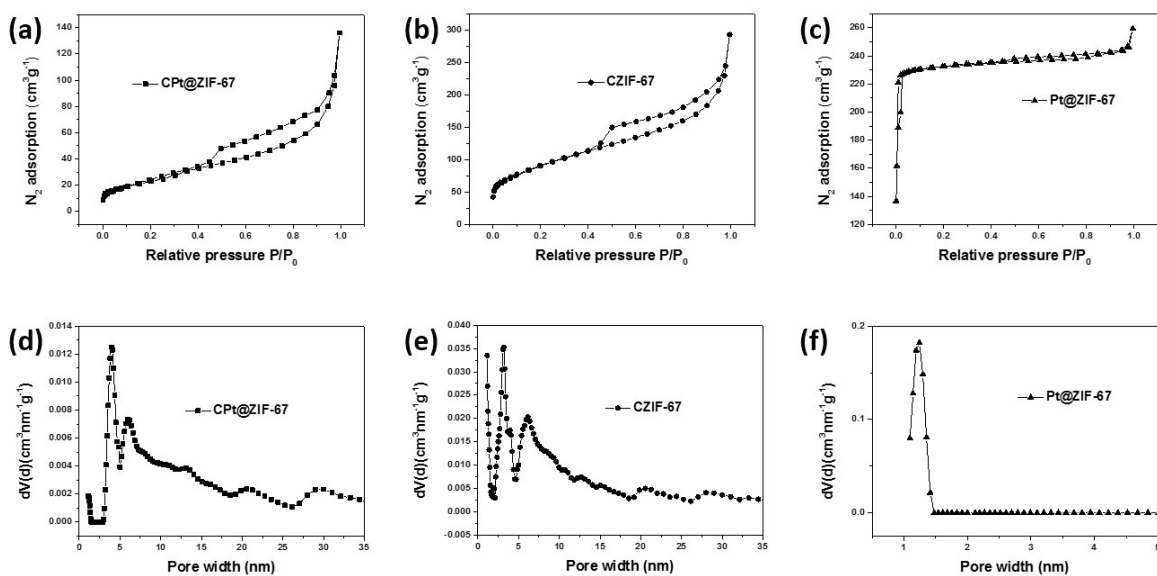

Fig. S11. N$_2$ sorption isotherms of (a) CPt@ZIF-67, (b) CZIF-67 and (c) Pt@ZIF-67. The pore size distribution of (d) CPt@ZIF-67, (e) CZIF-67 and (f) Pt@ZIF-67.
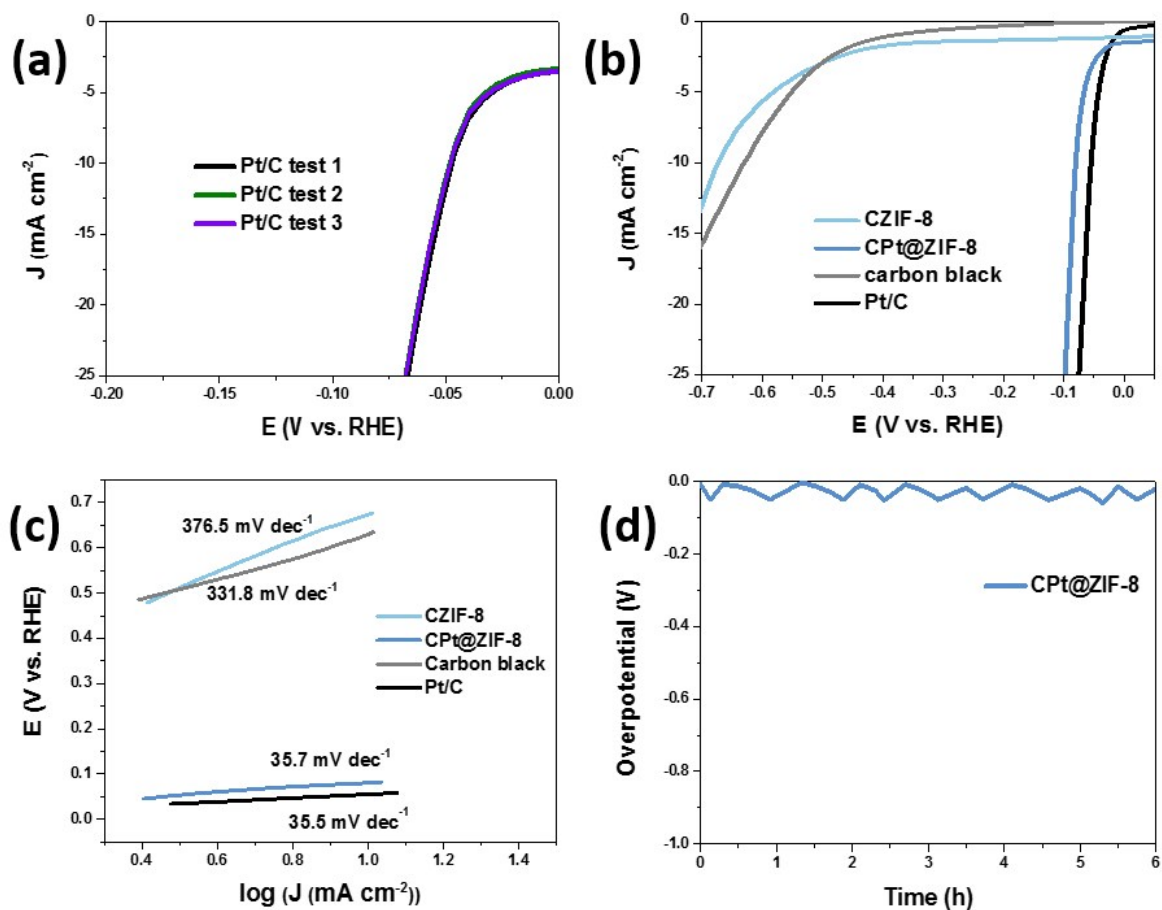
Fig. S12. (a) Polarization curves of three tests for 20 wt% Pt/C. (b) Polarization curves of CZIF-8, CPt@ZIF-8, carbon black and 20 wt% Pt/C. (c) Tafel plots of CZIF-8, CPt@ZIF-8, carbon black and 20 wt% Pt/C. (d) Chronopotentiometry of CPt@ZIF-8 under the current density of 10 mAcm^{-2} up to 6 hours.
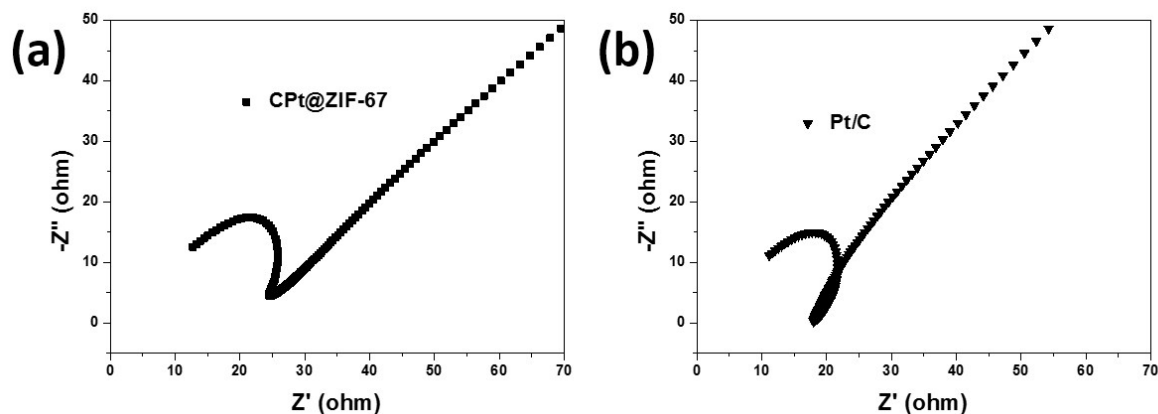
Fig. S13. Electrochemical impedance spectra (EIS) of (a) CPt@ZIF-67 and (b) commercial 20 wt% Pt/C over the frequency ranging from 100 kHz to 00.1 Hz at the open-circuit voltage.
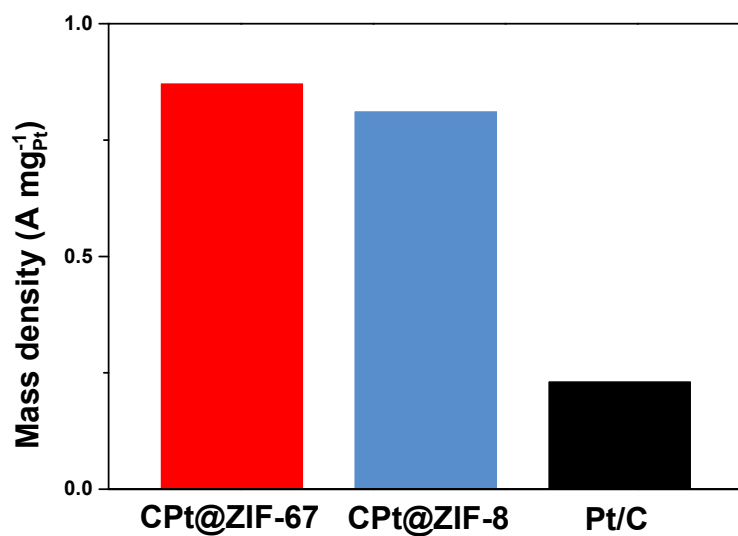
Fig. S14. Mass activity at 0.01 V (versus RHE) of the CPt@ZIF-67, CPt@ZIF-8 and Pt/C catalysts for the HER.

Co₅₅   Pt@Co54   2Pt@Co53

Fig. S15. The Co_{55} (a), $PtCo_{54}$ (b) and Pt_2Co_{53} (c) metal clusters. Each cluster optimised to energy minimum.

C_{240} Pt@Co@C

- H5
- H6_1
- H6_2

- T
- H5_1
- H5_2
- H6_1
- H6_2
- H6_3

Fig. S16. The possible reactive sites of C_{240} and C_{240} with Pt/Co alloy cluster inside.

Fig. S17. The free energy diagram of naked Co and Pt/Co alloy clusters.

Table S1. Three main industrial pathway for hydrogen production.

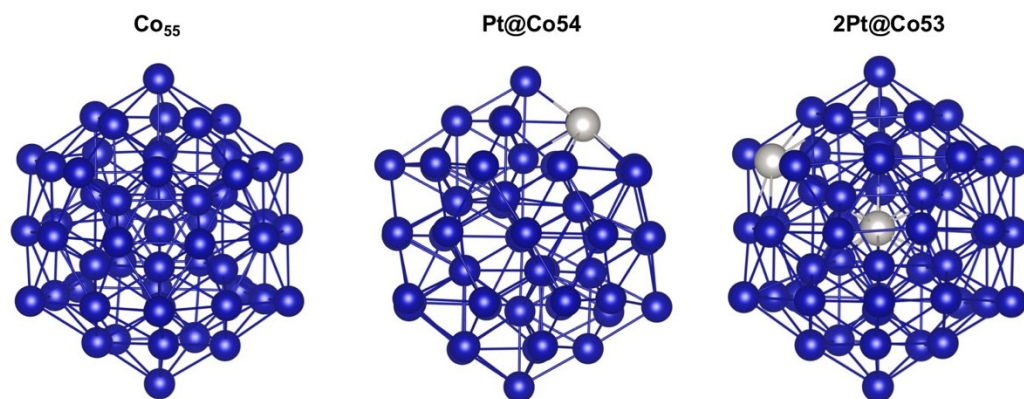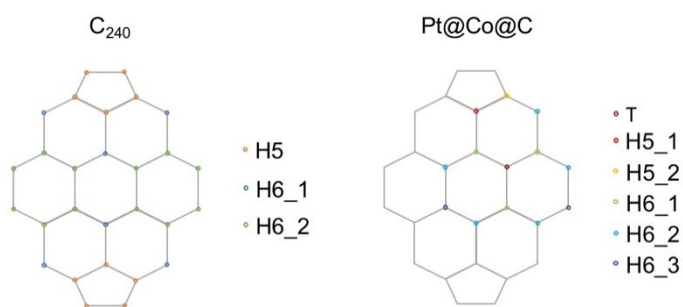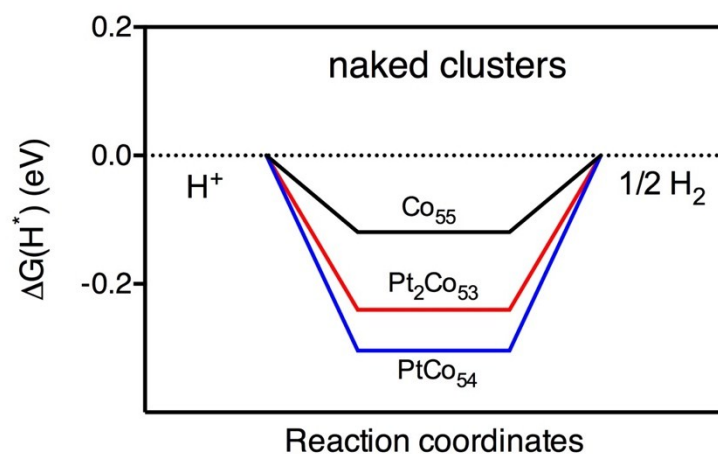| Method	Reagents	Products	Main reaction pathway
Steam methane reforming	Methane and steam	H_2 and CO_2	$CH_4 + 2H_2O \rightarrow 4H_2 + \mathbf{CO_2}$
Coal gasification	Coal and steam	H_2 and CO_2	$C + 2H_2O \rightarrow 2H_2 + \mathbf{CO_2}$
Water electrolysis	Water and electricity	H_2 and O_2	$2H_2O \rightarrow 2H_2 + O_2$

Table S2. Average bond length of C-N in pyrrole and pyridine.[6]

Chemical class	Structure formula	Average C-N bond length (Å)
Pyrrole		1.372
Pyridine		1.337
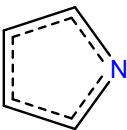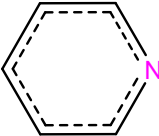
Table S3. Pt content in CPt@ZIF-67.

Atomic weight percentage from XPS	Weight percentage of Pt in the catalyst
0.05	0.70
0.06	0.85
0.06	0.90
0.07	0.99
0.07	1.01
0.08	1.15
Average	0.93

Table S4. TOF of the CPt@ZIF-67 and other catalysts.

Catalysts	Electrolyte	Overpotential (mV)	TOF (s^{-1})	Reference
CPt@ZIF-67	0.5 M H_2SO_4	100	2.94	This work
Li-PPS ND	0.5 M H_2SO_4	140	1.60	7
MoS_2|Au111]	0.5 M H_2SO_4	100	~0.10	8
FeP/Ti	0.5 M H_2SO_4	100	0.28	9
Ni-C-N NSs	0.5 M H_2SO_4	100	0.44	10
CoP	0.5 M H_2SO_4	100	0.046	11
CoN_x/C	0.5 M H_2SO_4	100	0.39	12
Ni_2P nanoparticles	0.5 M H_2SO_4	100	0.015	13
Electrodeposited H_2-CoCat	aqueous phosphate buffer	380	0.020	14
Defect-rich MoS_2 nanosheet	0.5 M H_2SO_4	300	0.73	15

Table S5. The calculated formation energy of single Pt atom doping in Co_{55} cluster.

Pt doping position	E formation (eV)
corner	-1.13
edge	-1.28
body	2.96

Table S6. The calculated formation energy of dual Pt atoms doping in C_{55} cluster.

Pt doping position	E formation (eV)
corner- corner nearby	-5.49
corner- corner faraway	-5.59
corner- edge nearby	-4.57
corner- edge faraway	-5.69
corner- body	-5.47
edge- edge nearby	-5.63
edge-edge faraway	-5.47
edge- body	-5.78
body-body nearby	-5.17
body-body faraway	-4.95

Note 1.

To calculate the turnover frequency (TOF) per platinum site on the CPt@ZIF-67 catalyst, we used the following formula:

$$TOF = \frac{\text{\# total hydrogen turnover} / cm^2 \text{ geometric area}}{\text{\# active sites} / cm^2 \text{ geometric area}}$$

The maximum number of the active sites was calculated based on the assumption that all Pt atoms in the CPt@ZIF-67 form the active sites and are accessible to the electrolyte. The Pt content of the CPt@ZIF-67 was calculated from the ICP data:

$$\frac{5\ mg}{100\ mg} \times 0.26\frac{mg}{cm^2} \times \frac{1}{195.08}\frac{mmol}{mg} \times 6.022 \times 10^{20}\frac{sites}{mmol} = 4.01 \times 10^{16}\frac{sites}{cm^2}$$

The total number of hydrogen turnover was calculated from the current density:

$$\#_{H_2} = \frac{j \times N_A}{n \times F}$$

j = the current density (A cm^2)

N_A = the Avogadro number

n = the number of electrons transferred to evolve H_2

F = the Faraday constant

$$\#_{H_2}$$
$$= (j\frac{mA}{cm^2})(\frac{1\ mol\ e^{-1}}{96485.3\ C})(\frac{\frac{1C}{s}}{1000mA})(\frac{1molH_2}{2mol\ e^{-1}})(\frac{6.022 \times 10^{23}molecu}{1mol\ H_2}$$
$$10^{23}\frac{H_2/s}{cm^2}per\frac{mA}{cm^2}$$

Hence, at an overpotential of 100 mV, the HER current density is 37.8 mA cm-2, and the TOF of the CPt@ZIF-67 was

$$TOF = \frac{\frac{3.12 \times 10^{15}H_2/s}{cm^2}per \times 37.8\frac{mA}{cm^2}}{4.01 \times 10^{16}\ sites\ per\ cm^2} = 2.94\ s^{-1}$$

Similarly, the TOF of the CPt@ZIF-67 at the overpotential of 50 mV was

$$TOF = \frac{\dfrac{3.12 \times 10^{15} H_2/s}{cm^2} per \times 10.3 \dfrac{mA}{cm^2}}{4.01 \times 10^{16} \, sites \, per \, cm^2} = 0.80 \, s^{-1}$$

Note 2.

Cyclic voltammetry (CV) measurements were carried out in 0.5 M H_2SO_4 electrolyte at a scan rate of 10 mVs^{-1}. The ECSA was determined by the following formula:

specific ECSA = Q_H / (m × q_H)

where Q_H is the total charge for H_{upd} adsorption, m is the active mass of Pt metal, and q_H is the charge required to oxidize a monolayer of hydrogen on a Pt surface.

The ECSA was estimated by measuring the coulombic charge for hydrogen adsorption (Q_H) in the range of -0.2 to -0.4 V (vs. RHE) and q_H is a constant which equals to 210 μC cm^{-2}. The H_{upd} adsorption charge (Q_H) can be calculated by $Q_H = Q/2$, where Q is the total charge under the H_{upd} adsorption/desorption area obtained after double-layer correction. The loading mass of Pt was investigated by the microwave plasma atomic emission spectroscopy (MP-AES) result. Hence, the ECSA of CPt@ZIF-67 is 64.3 m^2 g-1 pt.

Note 3.

ZIF-8 was synthesized using a similar synthetic route with ZIF-67, Pt@ZIF-8 and CPt@ZIF-8 only using the zinc nitrate hexahydrate, instead of the cobalt nitrate hexahydrate.

Before annealing, the AFM imaging and height profile measurements indicate the cubic structure of Pt@ZIF-8 and the particle sizes of Pt@ZIF-8 can vary from 200 to 400 nm (Fig. S2d-f). The SEM images (Fig. S3a) confirms the same morphology.

After annealing, CZIF-8 showed no evident peak, implying an amorphous structure. It also confirmed that there is virtually no crystalline Zn residue for ZIF-8 related compounds after annealing at 900 °C or above. For the CPt@ZIF-8, the peak at 40.7° can be assigned to Pt (111)

(JCPDS 65-2868), which also possesses the active sites and lowers the overpotential for HER (Fig. S8d).

The LSV curve of CPt@ZIF-8 was shown in Fig. S11a, along with those of CZIF-8, carbon black and 20 wt% Pt/C for comparison. Overall, the catalysts with Pt loading outperform those without. The similar performance levels of the CZIF-8 and carbon black also indicate no metal residue as catalysts centres in the CZIF-8. Tafel slope of the four samples were plotted in Fig. S11b. The values are 376.5, 35.7, 331.8 and 38.1 mV dec^{-1} for CZIF-8, CPt@ZIF-8, carbon black and 20 wt% Pt/C, respectively. The results indicate that the HER follows the Volmer-Heyrovsky mechanism.[16,17] It demonstrates the same trend as in the polarization curves. Both CPt@ZIF-8 has a comparable HER activity with the commercial 20 wt% Pt/C. In addition, an 6-hour stability test of CPt@ZIF-8 was carried out, as shown in Fig. S11c, where the activity decays are virtually negligible. This could be attributed to the catalyst being protected by the carbon shell from erosion by the acidic electrolyte.

References

(1) S. Gadipelli, T. Zhao, S. A. Shevlin and Z. Guo, *Energy Environ. Sci.* 2016, **9**, 1661–1667.

(2) K. S. Park, Z. Ni, A. P. Côté, J. Y. Choi, R. Huang, F. J. Uribe-Romo, H. K. Chae, M. O'Keeffe and O. M. Yaghi, *Proc. Natl. Acad. Sci.* 2006, **103**, 10186–10191.

(3) Z. Hu and M. P. Srinivasan, *Microporous Mesoporous Mater.* 2001, **43**, 267–275.

(4) P. T. Hsieh, Y. C. Chen, K. S. Kao and C. M. Wang, *Appl. Phys. A Mater. Sci. Process.* 2008, **90**, 317–321.

(5) T. Yu, Y. Zhu, X. Xu, Z. Shen, P. Chen, C. T. Lim, J. T. L. Thong and C. H. Sow, *Adv. Mater.* 2005. 2005, **17**, 1595–1599.

(6) F. H. Allen, O. Kennard, D. G. Watson, L. Brammer, A. G. Orpen and R. Taylor, *J. Chem.*

Soc. Perkin Trans. 2 1987, **S1**, 1695–1914.

(7) X. Zhang, Z. Luo, P. Yu, Y. Cai, Y. Du, D. Wu, S. Gao, C. Tan, Z. Li, M. Ren, T. Osipowicz, S. Chen, Z. Jiang, J. Li, Y. Huang, J. Yang, Y. Chen, C. Y. Ang, Y. Zhao, P. Wang, L. Song, X. Wu, Z. Liu, A. Borgna and H. Zhang, *Nat. Catal.* 2018, **1**, 460–468.

(8) T. F. Jaramillo, K. P. Jorgensen, J. Bonde, J. H. Nielsen, S. Horch and I. Chorkendorff, *Science* 2007, **317**, 100–102.

(9) J. F. Callejas, J. M. McEnaney, C. G. Read, J. C. Crompton, A. J. Biacchi, E. J. Popczun, T. R. Gordon, N. S. Lewis and R. E. Schaak, *ACS Nano* 2014, **8**, 11101–11107.

(10) J. Yin, Q. Fan, Y. Li, F. Cheng, P. Zhou, P. Xi and S. Sun, *J. Am. Chem. Soc.* 2016, **138**, 14546–14549.

(11) E. J. Popczun, C. G. Read, C. W. Roske, N. S. Lewis and R. E. Schaak, *Angew. Chemie - Int. Ed.* 2014, **53**, 5427–5430.

(12) H.-W. Liang, S. Brüller, R. Dong, J. Zhang, X. Feng and K. Müllen, *Nat. Commun.* 2015, **6**, 7992–7999.

(13) E. J. Popczun, J. R. McKone, C. G. Read, A. J. Biacchi, A. M. Wiltrout, N. S. Lewis and R. E. Schaak, *J. Am. Chem. Soc.* 2013, **135**, 9267–9270.

(14) S. Cobo, J. Heidkamp, P. A. Jacques, J. Fize, V. Fourmond, L. Guetaz, B. Jousselme, V. Ivanova, H. Dau, S. Palacin, M. Fontecave and V. Artero, *Nat. Mater.* 2012, **11**, 802–807.

(15) J. Xie, H. Zhang, S. Li, R. Wang, X. Sun, M. Zhou, J. Zhou, X. W. Lou and Y. Xie, *Adv. Mater. Adv. Mater.* 2013, **25**, 5807–5813.

(16) M. Zeng and Y. Li, *J. Mater. Chem. A* 2015, **3**, 14942–14962.

(17) Y. Zheng, Y. Jiao, Y. Zhu, L. H. Li, Y. Han, Y. Chen, A. Du, M. Jaroniec and S. Z. Qiao, *Nat. Commun.* 2014, **5**, 1–8.